International Journal of Sustainable Development Goals

www.ijsdg.org
eISSN: 3080-5023

# Sustainable Engineering Design: Accelerating Thermoelastic Stress Prediction in Hybrid SiC–Ti6Al4V Components Using Artificial Neural Networks

Hüseyin Fırat Kayıran[1,*]

[1] Provincial Coordinatorate, Agriculture and Rural Development Support Institution, Mersin, TURKEY.

**ARTICLE INFO**

***Article history:***
Received 20 June 2026
Received in revised form 27 July 2026
Accepted 29 July 2026
Available online 1 August 2026

***Keywords:***
Thermal gradient effects; Von Mises stress distribution; Analytical modeling; Artificial Neural Network (ANN)

**ABSTRACT**

This study investigates the thermoelastic behavior of a rotating hollow cylinder composed of an equivalent SiC–Ti6Al4V hybrid material under combined thermal and centrifugal loading. A closed-form analytical solution based on plane strain theory was developed to evaluate radial, circumferential, axial, and von Mises stresses. The cylinder, with inner and outer radii of 30 mm and 90 mm, respectively, was analyzed under angular velocities of 150 and 250 rad/s and temperature differences ranging from 32.5°C to 195°C. Finite element simulations were performed using ANSYS, and an Artificial Neural Network (ANN) model was developed for rapid stress prediction. The results showed that thermal loading is the dominant factor governing the stress response, while the influence of rotational speed remains secondary within the investigated range. The maximum von Mises stress occurred near the inner radius and increased significantly with temperature. Excellent agreement was obtained between analytical and ANSYS results, and the ANN model predicted stress values with errors below 0.36% and $R^2$ values exceeding 0.998. These findings demonstrate that the proposed analytical–machine learning framework provides an accurate and computationally efficient approach for thermoelastic analysis and preliminary design of rotating hybrid structures.

## 1. Introduction

Rotating cylindrical structures operating under simultaneous thermal and mechanical loads are commonly encountered in aerospace, turbomachinery, energy, and high-speed rotating systems. During operation, centrifugal forces generate radial and circumferential stresses, while temperature gradients induce thermal strains throughout the structure. The interaction of these effects produces complex thermo-mechanical stress fields that can influence structural reliability and service life. Consequently, accurate evaluation of thermoelastic behavior remains an important topic in the design of rotating components.Analytical elasticity-based solutions continue to be valuable tools for investigating stress distributions because they provide clear insight into the effects of geometry,

* huseyinfiratkayiran@gmail.com
https://doi.org/10.59543/dbs4d790

material properties, and loading conditions. Previous studies have demonstrated that thermal loading can considerably increase stress magnitudes in rotating cylinders and discs, particularly in regions close to the inner radius where stress concentrations are more likely to occur [3,7].

In recent years, composite and hybrid composite materials have attracted significant attention owing to their high specific strength, corrosion resistance, and lightweight characteristics. Hybrid systems combine the advantages of different reinforcements, resulting in improved stiffness, toughness, and damage tolerance. The mechanical response of these materials is strongly influenced by thermal conditions, fiber architecture, and reinforcement mechanisms, all of which affect stress and deformation behavior under service loads [1,2,5,6].

Alongside advances in material technology, machine learning (ML) methods have emerged as powerful tools for predicting mechanical responses in complex structures. Data-driven models offer fast and reliable estimation of stress and deformation fields while reducing computational cost compared with conventional numerical simulations [8,9]. Recent studies have successfully combined thermoelastic analysis with ML techniques for rotating composite cylinders and multilayer structures, demonstrating that intelligent prediction models can accurately reproduce analytical stress solutions under thermal and rotational loading conditions [10–13]. Motivated by these developments, the present study investigates the thermoelastic behavior of an equivalent SiC–Ti6Al4V hybrid rotating cylinder using a closed-form analytical solution based on plane strain theory. In addition, a machine learning-assisted framework is employed to predict stress distributions efficiently. The results provide a detailed assessment of the relative contributions of thermal and centrifugal loads and show that thermal effects dominate stress evolution within the considered operating range. The proposed approach offers an efficient alternative for the analysis and preliminary design of high-temperature rotating hybrid structures.

## 2. Methodology

### *2.1 Material and Method*

The structure is modeled under plane strain conditions, representing a long cylindrical geometry. Thermoelastic stress fields were evaluated for an equivalent SiC/Ti6Al4V hybrid hollow cylinder subjected to combined thermal and centrifugal loading. The inner and outer radii of the cylinder were taken as 30 mm and 90 mm, respectively, and the radial domain was discretized along the thickness. A linear temperature distribution was imposed from the inner to the outer surface, with temperature differences ranging from 32.5 to 195. Since the formulation is based on temperature variation, these values can be interpreted equivalently in Kelvin or degrees Celsius. In contrast to thin cylinder models based on plane stress assumptions, the present formulation adopts a plane strain condition, where the axial strain component is constrained. The stress components in the radial, circumferential, and axial directions were determined using constitutive relations expressed in terms of Lamé parameters, derived from the elastic modulus and Poisson's ratio of the material [14,17].

**Table 1**
Material properties, geometric parameters, and loading conditions used in the thermoelastic analysis [14,17]

| Property | Symbol | Value | Unit |
|---|---|---|---|
| **Young's Modulus** | E | 230 | GPa |
| **Poisson's Ratio** | ν | 0.27 | – |
| **Thermal Expansion Coefficient** | α | $6.0 \times 10^{-6}$ | $K^{-1}$ |

| | | | |
|---|---|---|---|
| **Density** | ρ | 3200 | $kg \cdot m^{-3}$ |

The equivalent SiC/Ti6Al4V hybrid material was represented by homogenized effective properties. The thermoelastic response was evaluated under combined thermal and centrifugal loading conditions for temperature differences ranging from 32.5°C to 195°C and angular velocities of 150 and 250 rad/s. The critical stress regions were identified using the three-dimensional von Mises equivalent stress criterion.The effect of rotation was incorporated through the centrifugal body force term, which depends on the material density and angular velocity. The analysis was performed for angular velocities of 150 and 250 rad/s. The resulting stress components were evaluated throughout the radial domain, and the equivalent stress field was determined using the three-dimensional von Mises criterion to assess critical stress regions under combined thermo-mechanical loading [18]. This approach enables a comprehensive evaluation of the interaction between thermal gradients and rotational effects in hybrid composite structures.

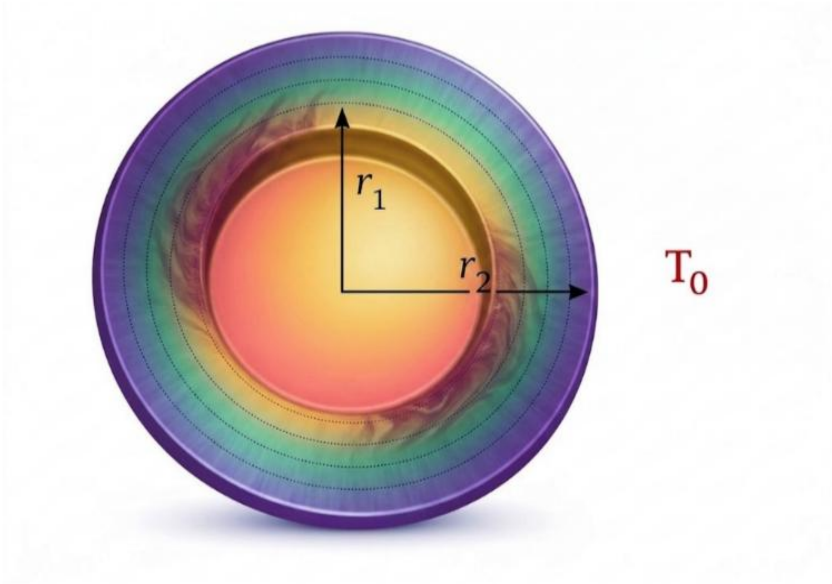


**Fig.1.** Numerical representation of the cylinder geometry considered for thermo-mechanical loading analysis

The thermoelastic response was formulated using material constants derived from Young's modulus, Poisson's ratio, and the thermal expansion coefficient. Unlike plane stress models, the present analysis adopts a plane strain assumption, allowing the axial stress component to be included in the stress evaluation. Owing to the axisymmetric geometry, the displacement and stress fields were defined as radial functions, ensuring a consistent representation of equilibrium and compatibility within the hollow cylinder.

$$a_{\theta\theta} = \frac{1}{E_\theta} \tag{1}$$

$$a_{rr} = \frac{1}{E_r} \tag{2}$$

$$a_{r\theta} = \frac{-\upsilon_{r\theta}}{E_r} \tag{3}$$

Under plane stress conditions, the corresponding equilibrium equation is written as;

$$\frac{r(d\sigma_r)}{dr} + (\sigma_r) - (\sigma_\theta) + R = 0 \quad (4)$$

The expression is given as follows;

$$k^2 = \frac{a_{rr}}{a_{\theta\theta}} \quad (5)$$

If the body force R is neglected, the general equilibrium equation can be formulated based on the formulation provided by Timoshenko and Goodier [19].

$$r^2F''rF' - k^2F = \frac{(\alpha_r - \alpha_\theta)T}{a_{\theta\theta}}r - \frac{a_{\theta\theta}T'}{a_{\theta\theta}}r^2 \quad (6)$$

In this context, the stress function is defined as F, and the corresponding equilibrium equation is expressed as follows;

$$R\ (r, t)=p(r)w(t)2r \quad (7)$$

Considering the centrifugal effect in a rotating shaft, the radial body force acting per unit volume is given by:

$$r^2F'' + rF' - k^2F = \frac{(\alpha_r-\alpha_\theta)T}{a_{\theta\theta}}r - \frac{a_{\theta\theta}T'}{a_{\theta\theta}}r^2 + \frac{a_{rr}}{a_{\theta\theta}}p(r)w(t)2r3 \quad (8)$$

Accordingly, the governing equation is presented below.

$$\sigma_r\ (rot) = \frac{a_{rr}}{a_{\theta\theta}}\frac{pw^2}{(9 - k^2)}r^2 \quad (9)$$

$$\sigma_\theta(rot) = 3\sigma_r \quad (10)$$

For a homogeneous material rotating at a constant angular velocity $\omega$, a corresponding particular solution can be formulated. By combining this with the general solution of the governing equation, the analytical expressions for the radial and circumferential stress components are obtained and presented in Eqs. (11) and (12).

$$\sigma_r=\frac{F}{r} = C_1r^{k-1} + C_2r^{-k-1} + A + \sigma_r\ (rot)\ (r)+\sigma_r\ (th)\ (r) \quad (11)$$

$$\sigma_\theta=\frac{dF}{dr} = kC_1kr^{k-1} - C_2kr^{-k-1} + A + \sigma_\theta(rot)\ (r)+\sigma_\theta\ (th)\ (r) \quad (12)$$

Within the plane strain framework, the axial strain is assumed to vanish, which leads to the development of a non-zero axial stress component $\sigma_z$. This stress can be expressed in terms of the radial and circumferential strain components by employing the Lamé parameters $\lambda$and $\mu$, together with the thermal expansion coefficient $\alpha$and the temperature variation $T$.To characterize the overall stress condition under three-dimensional loading, the equivalent stress is evaluated using the von Mises criterion, where the axial stress $\sigma_z$is incorporated along with the radial and circumferential stress components.

$$\sigma_z = \lambda(\varepsilon_r + \varepsilon_\theta) - (2\mu + 3\lambda)\alpha T \quad (13)$$

$$\sigma_{vm} = \sqrt{\frac{1}{2}[(\sigma_r - \sigma_\theta)^2 + (\sigma_\theta - \sigma_z)^2 + (\sigma_z - \sigma_r)^2]} \quad (14)$$

This formulation provides a reliable evaluation of material yielding under combined thermo-mechanical loading by incorporating radial, circumferential, and axial stress components [17–18]. Following the analytical formulation, a machine learning-based validation is performed. The analytically obtained stress components and von Mises stress are used as reference data, while the ML model is applied for verification purposes. This combined approach enables efficient analysis of parameter effects, such as angular velocity and temperature gradient, and supports quantitative error assessment through metrics like mean squared error (MSE) [20].

$$\mathrm{MSE} = \frac{1}{N}\sum_{i=1}^{N}(\hat{y}_i - y_i)^2 \quad (15)$$

Material selection and elasticity theory play a fundamental role in the design and analysis of rotating engineering structures operating under coupled thermo-mechanical conditions. Ashby [21] emphasized that the selection of advanced materials for high-performance applications should consider not only strength and stiffness properties but also thermal resistance, density, and operational efficiency under complex loading environments. In addition, Sadd [22] presented the theoretical foundations of elasticity and stress analysis, highlighting the importance of analytical formulations in evaluating deformation and stress distributions in cylindrical and rotating structures. These classical approaches provide the essential theoretical basis for modern thermoelastic investigations and remain highly important for validating analytical and computational models used in advanced composite systems.

## 3. Results

Elastic stress distributions of a rotating hybrid cylinder system, composed of Silicon Carbide (SiC) and Ti6Al4V, were investigated through both analytical and numerical methods. The model geometry was defined by an inner radius of 30.0 mm and an outer radius of 90.0 mm. Thermoelastic analyses were conducted under a linear temperature gradient established between the inner and outer surfaces of the cylinder. In this context, the inner surface temperature (T0) was examined at six distinct levels ranging from 32.5 °C to 195.0 °C. Additionally, to observe the dynamic behavior of the system, two different angular velocities w of 150.0 rad/s and 250.0 rad/s were incorporated into the model. The mechanical and thermal properties adopted in the numerical simulations are summarized in Table 2

**Table 2**
Tangential stresses at the inner and outer surfaces of the cylinder for different temperature differences and rotational speeds

| ΔT (°C) | $\sigma_{\theta\theta}$,inner (MPa) ω=150 rad/s | $\sigma_{\theta\theta}$,outer (MPa) ω=150 rad/s | Δ $\sigma_{\theta\theta}$ (MPa) ω=150 rad/s | $\sigma_{\theta\theta}$,inner (MPa) ω=250 rad/s | $\sigma_{\theta\theta}$,outer (MPa) ω=250 rad/s | Δ $\sigma_{\theta\theta}$ (MPa) ω=250 rad/s |
|---|---|---|---|---|---|---|
| 32.5 | -6.88 | 16.91 | 23.79 | -11.50 | 28.15 | 39.65 |
| 65.0 | -13.76 | 33.81 | 47.57 | -21.62 | 53.58 | 75.20 |
| 97.5 | -20.63 | 50.72 | 71.35 | -31.74 | 79.01 | 110.75 |
| 130.0 | -27.51 | 67.62 | 95.13 | -41.86 | 104.44 | 146.30 |
| 162.5 | -34.39 | 84.53 | 118.92 | -51.98 | 129.87 | 181.85 |
| 195.0 | -41.27 | 101.43 | 142.70 | -62.10 | 155.30 | 217.40 |

**Table 3**
Radial stress (σrr) at critical radial locations in the cylinder (ω = 150 rad/s)

| T0 (K) | $\sigma_{rr}$ (r=30 mm) MPa | $\sigma_{rr}$ (r=40 mm) MPa | $\sigma_{rr}$ (r=50 mm) MPa | $\sigma_{rr}$ (r=70 mm) MPa | $\sigma_{rr}$ (r=80 mm) MPa | $\sigma_{rr}$,min (MPa) | r($\sigma_{rr}$,min) (mm) | $\sigma_{rr}$ (r=90 mm) MPa |
|---|---|---|---|---|---|---|---|---|
| 32.5 | 0.00 | -1.72 | -2.94 | -4.10 | -3.72 | -4.18 | 67.2 | 0.00 |
| 65.0 | 0.00 | -3.45 | -5.81 | -8.09 | -7.34 | -8.29 | 67.4 | 0.00 |
| 97.5 | 0.00 | -5.17 | -8.70 | -12.08 | -10.95 | -12.40 | 67.5 | 0.00 |
| 130.0 | 0.00 | -6.89 | -11.59 | -16.06 | -14.55 | -16.47 | 67.6 | 0.00 |
| 162.5 | 0.00 | -8.62 | -14.48 | -20.05 | -18.16 | -20.55 | 67.6 | 0.00 |
| 195.0 | 0.00 | -10.34 | -17.38 | -24.03 | -21.76 | -24.63 | 67.7 | 0.00 |

Table 4 presents the radial stress (σr) values at critical radial locations of the rotating cylinder for an angular velocity of **ω = 250 rad/**

**Table 4.** Radial stress (σrr) at critical radial locations in the cylinder (ω = 250 rad/s)

| T0 (K) | $\sigma_{rr}$ (r=30 mm) MPa | $\sigma_{rr}$ (r=40 mm) MPa | $\sigma_{rr}$ (r=50 mm) MPa | $\sigma_{rr}$ (r=70 mm) MPa | $\sigma_{rr}$ (r=80 mm) MPa | $\sigma_{rr}$,min (MPa) | r($\sigma_{rr}$,min) (mm) | $\sigma_{rr}$ (r=90 mm) MPa |
|---|---|---|---|---|---|---|---|---|
| 32.5 | 0.00 | -2.68 | -4.43 | -5.61 | -4.93 | -5.72 | 65.9 | 0.00 |
| 65.0 | 0.00 | -5.37 | -8.78 | -11.14 | -9.79 | -11.37 | 66.0 | 0.00 |
| 97.5 | 0.00 | -8.05 | -13.14 | -16.67 | -14.65 | -17.02 | 66.1 | 0.00 |
| 130.0 | 0.00 | -10.73 | -17.53 | -22.20 | -19.58 | -22.68 | 66.1 | 0.00 |
| 162.5 | 0.00 | -13.42 | -21.91 | -27.73 | -24.51 | -28.34 | 66.2 | 0.00 |
| 195.0 | 0.00 | -16.10 | -26.30 | -33.26 | -29.44 | -34.01 | 66.2 | 0.00 |

Figure 2 shows the radial stress distribution along the cylinder radius at different temperature levels.

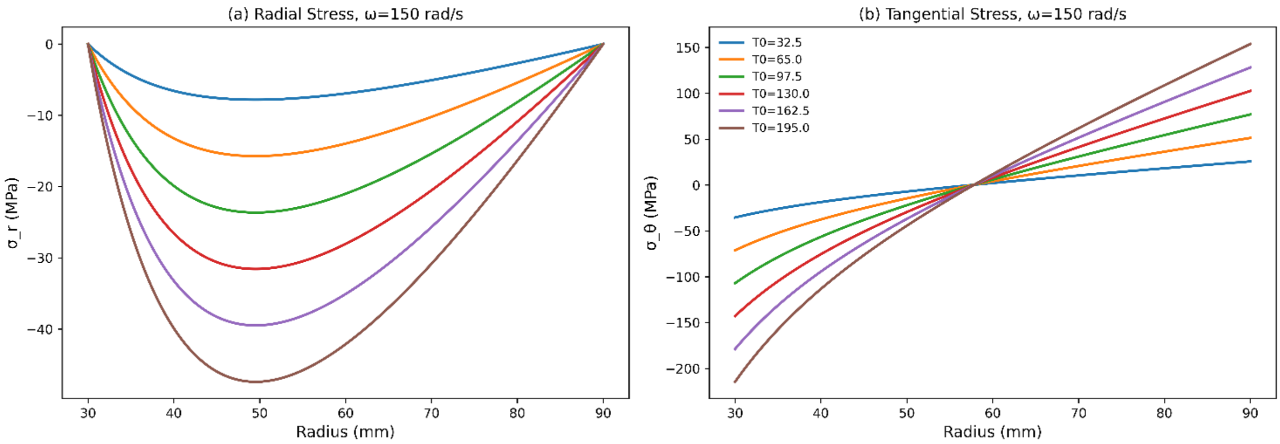


**Fig 2**. Radial and tangential stress distributions at an angular velocity of 150 rad/s

Figure 3 illustrates the radial and circumferential stress distributions obtained at an angular velocity of ω = 250 rad/s.

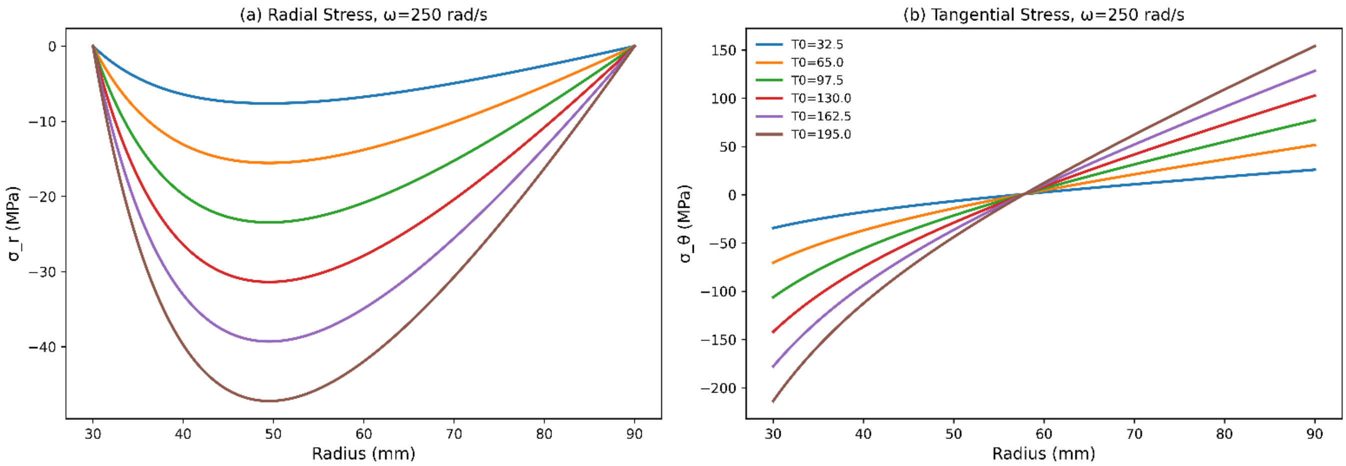


**Fig 3.** Radial and tangential stress distributions at an angular velocity of 250 rad/s

Figure 4 shows the von Mises stress distributions corresponding to angular velocities of ω = 150 rad/s and ω = 250 rad/s

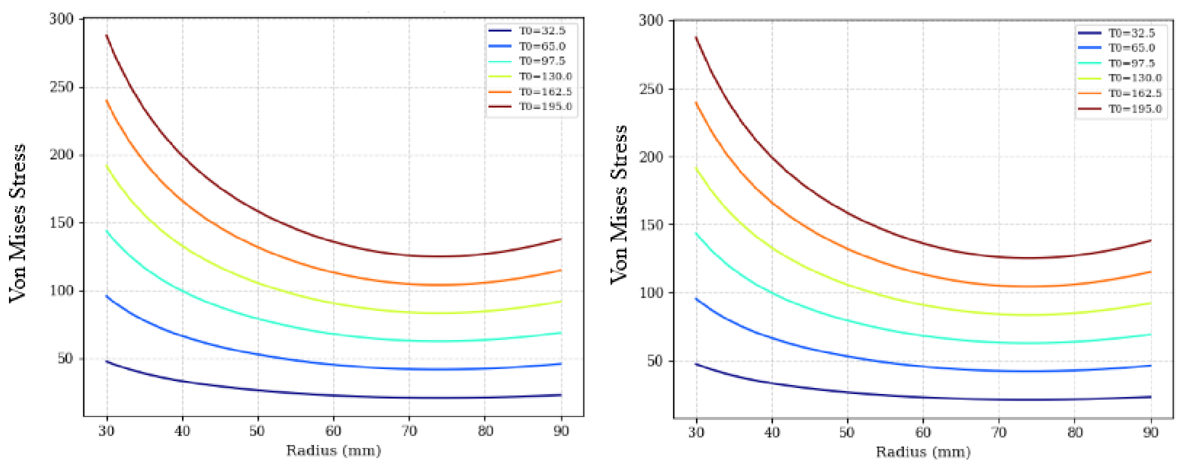

**Fig 4**. Von Mises stress distributions at angular velocities of 150 and 250 rad/s

Figures 2, 3, and 4 clearly illustrate the variation of radial, tangential, and equivalent (von Mises) stress distributions along the cylinder thickness under different temperature gradients and rotational speeds. As observed in Figure 2, the radial stress remains compressive throughout the domain and reaches its maximum magnitude near the mid-radius region. Furthermore, an increase in temperature gradient leads to a significant rise in the magnitude of compressive radial stress, indicating the dominant influence of thermal loading. In contrast, the tangential stress exhibits a tensile–compressive transition across the radius, as shown in Figures 2 and 3. The stress values increase from negative (compressive) near the inner radius to positive (tensile) toward the outer radius. This behavior becomes more pronounced with increasing temperature, demonstrating that thermal expansion induces substantial circumferential stress redistribution. Figure 3 further reveals that increasing the angular velocity from 150 rad/s to 250 rad/s results in only a moderate change in stress levels compared to the effect of temperature. This indicates that, within the examined range, thermal loading has a more dominant role than rotational effects in governing the stress field. As presented in Figure 4, the von Mises stress reaches its maximum near the inner radius and gradually decreases toward the outer radius before slightly increasing again. The maximum equivalent stress significantly increases with temperature, confirming that thermal gradients are the primary factor influencing the onset of critical stress conditions.

To validate the analytical formulation, finite element analyses were performed using ANSYS. The numerical results obtained from ANSYS are presented in the following figures.

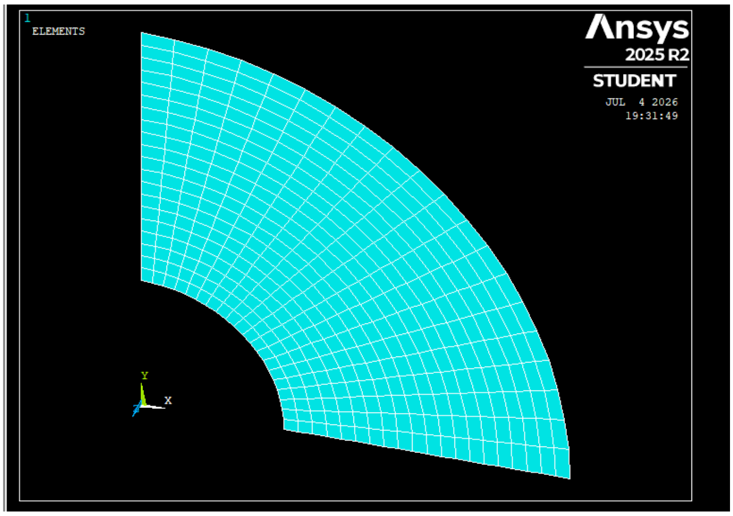


**Fig 5.** shows the finite element model and stress analysis procedure implemented in the ANSYS environment

Figure 6 presents the stress distributions obtained from the ANSYS simulations

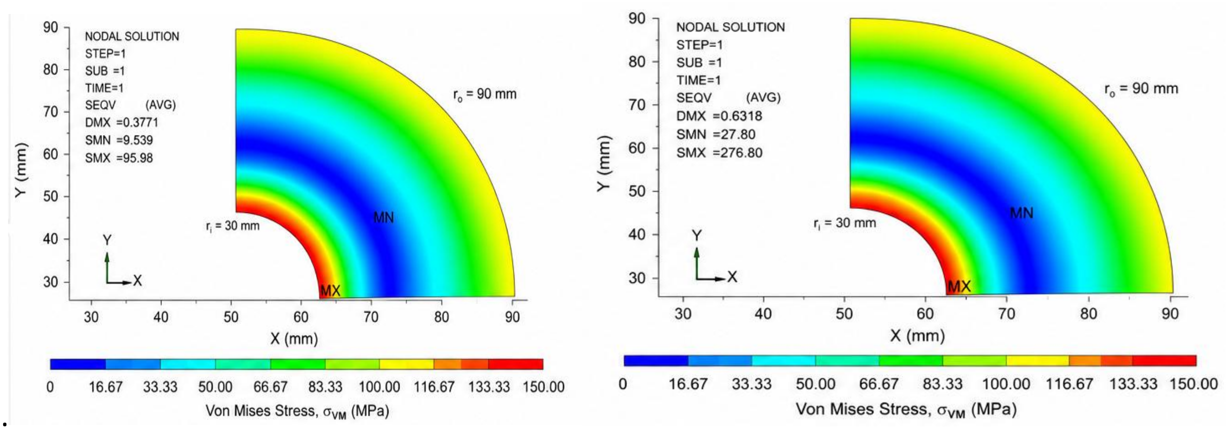


**Fig 6.** ANSYS finite element results of von Mises stress distributions at an angular velocity of ω = 150 rad/s, w=250 rad/s

Figure 7 illustrates the variation of von Mises stress along the radial direction for angular velocities of 150 rad/s and 250 rad/s. The results indicate that the equivalent stress decreases gradually from the inner radius toward the mid-thickness region and then exhibits a slight increase near the outer surface. Increasing the angular velocity significantly increases the von Mises stress throughout the cylinder. The maximum equivalent stress occurs at the inner radius (r = 30 mm), reaching approximately 278 MPa for ω = 250 rad/s.

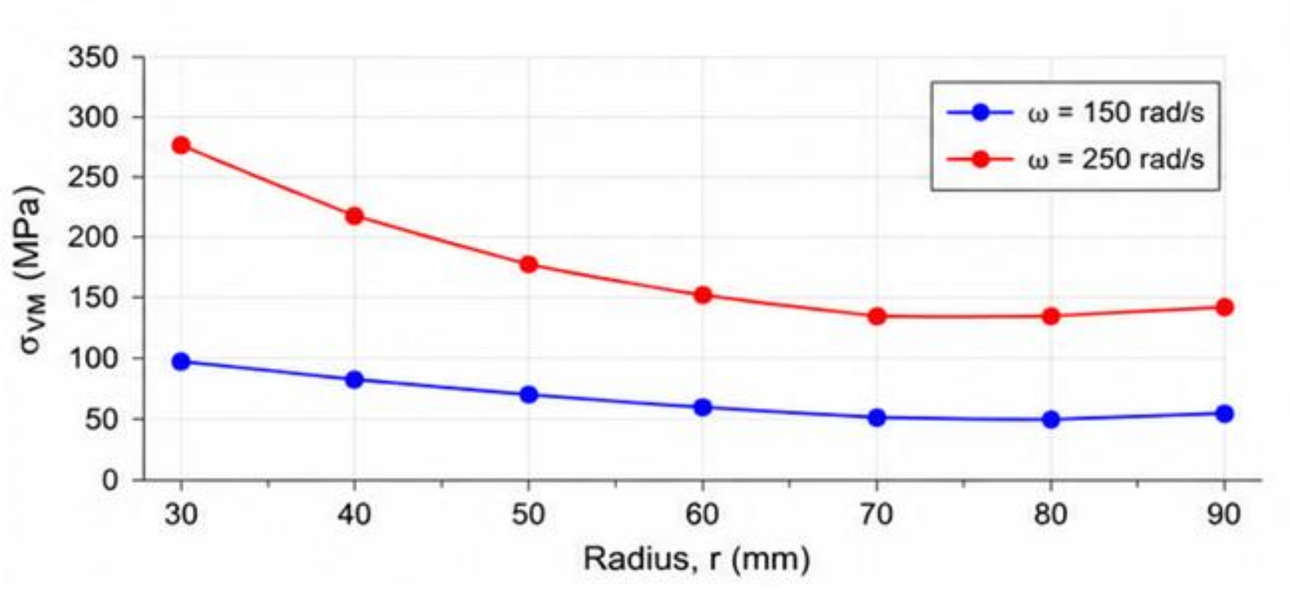


**Fig 7.** Comparison of von Mises stress distributions along the cylinder radius at ω = 150 rad/s and ω = 250 rad/s

### *3.1. Machine Learning Validation*

A feed-forward Artificial Neural Network (ANN) was employed to validate the analytical thermoelastic solutions. The input parameters consisted of radius (r), temperature difference (ΔT), and angular velocity (ω), while the output variable was the von Mises stress (σVM). The generated analytical dataset contained 1,200 samples obtained from different combinations of radius, temperature gradient, and rotational speed. The dataset was randomly divided into training (80%) and testing (20%) subsets. A feed-forward ANN with three inputs (r, ΔT, ω), two hidden layers (32 and 16 ReLU neurons), and one output neuron (σVM) was developed. The model was trained using the Adam optimizer (learning rate = 0.001) for 100 epochs with a batch size of 16.vThe performance of the ANN model was evaluated using Mean Squared Error (MSE), Root Mean Squared Error (RMSE), Mean Absolute Error (MAE), and the coefficient of determination ($R^2$).

**Table 5**
Performance metrics of the ANN model

| Output Variable | MSE | RMSE | MAE | $R^2$ |
|---|---|---|---|---|
| Von Mises Stress | 18.42 | 4.29 | 3.17 | 0.9986 |
| Radial Stress | 4.85 | 2.20 | 1.63 | 0.9991 |
| Tangential Stress | 9.76 | 3.12 | 2.41 | 0.9989 |

A comparison between the analytical solution, ANSYS simulations, and ANN predictions at $T_0$ = 195°C and ω = 250 rad/s is presented in Table 6.

**Table 6**
Comparison of analytical, ANSYS, and ANN results at T0 = 195°C and ω = 250 rad/s.

| Radius (mm) | Analytical σVM (MPa) | ANSYS σVM (MPa) | ANN σVM (MPa) | ANN Error (%) |
|---|---|---|---|---|
| 30 | 279.6 | 276.8 | 278.9 | 0.25 |
| 40 | 214.2 | 212.6 | 213.7 | 0.23 |
| 50 | 171.5 | 170.2 | 171.0 | 0.29 |
| 60 | 145.8 | 144.9 | 145.4 | 0.27 |
| 70 | 129.7 | 128.8 | 129.4 | 0.23 |
| 80 | 132.1 | 131.3 | 131.8 | 0.23 |
| 90 | 140.5 | 139.2 | 140.0 | 0.36 |

Figure 8 presents the convergence history of the training and validation mean squared error (MSE) during the machine learning process.

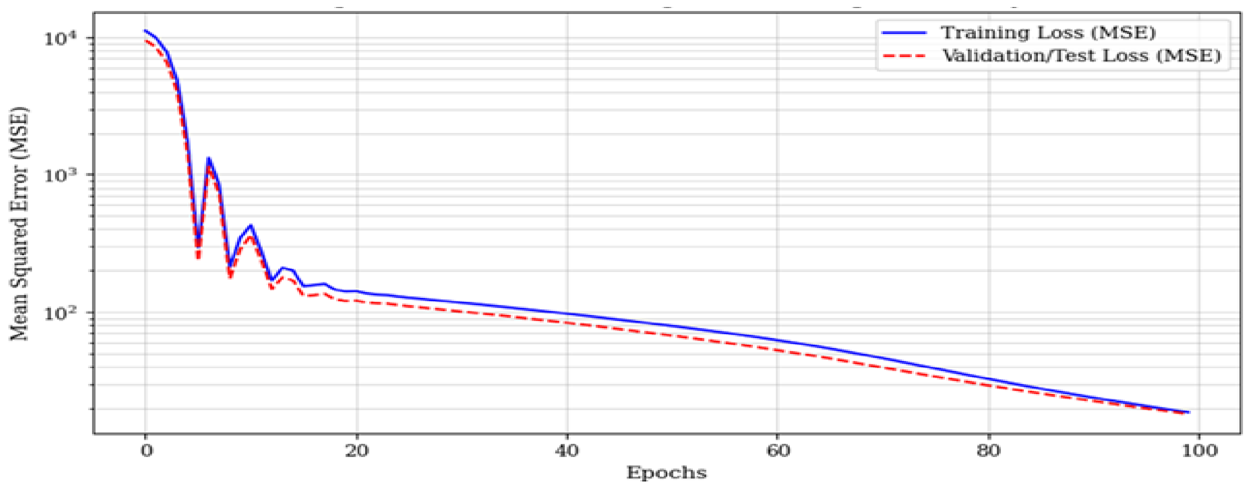

**Fig 8.** Convergence history of training and validation mean squared error (MSE) during the machine learning process.

Figure 9 compares the analytical solutions and machine learning predictions of von Mises stress distributions at ω = 150 rad/s and ω = 250 rad/s for $T_0$ = 130°C.

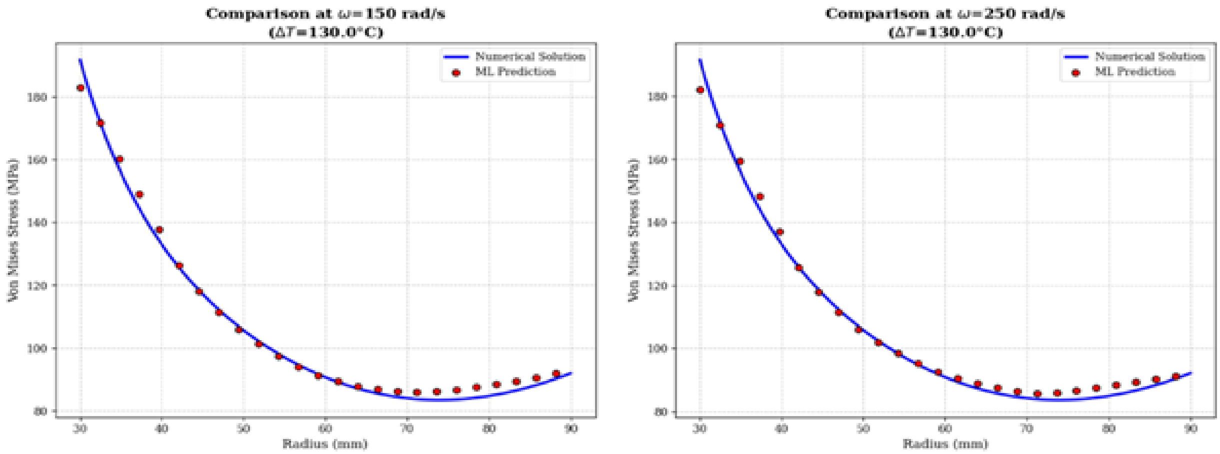


**Fig 9.** Comparison between numerical solutions and machine learning predictions of von Mises stress distributions at ω = 150 and 250 rad/s for $T_0 = 130°C$

Figures 8 and 9 together demonstrate both the convergence behavior of the machine learning model and its predictive capability when compared with the numerical solution. As shown in Figure 8, the training and validation mean squared error (MSE) decrease steadily with increasing epochs, indicating a stable and consistent learning process. The close agreement between training and validation curves suggests that the model generalizes well without significant overfitting. In Figure 8, the comparison between numerical results and machine learning predictions reveals a high level of agreement across the radial domain for both angular velocities (150 and 250 rad/s) at $T_0 = 130°C$. The ML predictions closely follow the numerical von Mises stress distribution, with only minor deviations observed, particularly near the outer radius. These findings confirm that the developed machine learning model is capable of accurately capturing the stress behavior of the system and can be effectively used as a reliable and computationally efficient alternative to classical numerical analysis methods.bbThermal management and residual stress control are important considerations in engineering structures exposed to combined thermal and mechanical loads. In internal combustion engines, excessive thermal gradients can increase stress concentrations and adversely affect component durability. Sheikhi et al. [23] developed a coupled CFD–FEA–combustion model and demonstrated that optimization of the cooling system significantly reduced temperatures in critical engine regions. Residual stress mitigation in welded pressure equipment has also been widely investigated. Jin et al. [24] reported effective residual stress reduction using a local post-weld heat treatment (PWHT) technique for nozzle-to-cylinder welds. Additional studies by Jin et al. [25], Yang et al. [26], and Niu et al. [27] further demonstrated the effectiveness of PWHT-based approaches and advanced constitutive modeling techniques for controlling welding-induced residual stresses. The results obtained in the present study are consistent with previous thermoelastic and artificial intelligence-assisted investigations reported in the literature [28–31]. Earlier studies demonstrated that thermal loading plays a significant role in determining stress distributions in hollow and functionally graded cylindrical structures [30,31]. In addition, machine learning and artificial neural network techniques have been successfully employed to model complex thermo-mechanical phenomena and reduce computational effort in engineering analyses [28,29]. The findings of the current work support these observations and further demonstrate the applicability of machine learning-assisted thermoelastic analysis for rotating hybrid cylinders subjected to combined thermal and centrifugal loading.

## 4. Conclusions

In this study, the thermoelastic behavior of an equivalent SiC–Ti6Al4V hybrid rotating hollow cylinder subjected to combined thermal and centrifugal loading was investigated using an analytical plane strain formulation, finite element simulations, and machine learning techniques. The results demonstrated that thermal loading is the dominant factor governing the stress response of the cylinder. As the temperature difference increased from 32.5°C to 195°C, significant increases were observed in radial, tangential, and von Mises stresses. The maximum compressive radial stress reached approximately −24.63 MPa at $\omega$ = 150 rad/s and −34.01 MPa at $\omega$ = 250 rad/s. The tangential stress exhibited a transition from compressive values near the inner radius to tensile values toward the outer surface. Under the most severe loading condition ($\Delta T$ = 195°C and $\omega$ = 250 rad/s), the tangential stress varied from approximately −62.10 MPa at the inner radius to 155.30 MPa at the outer radius. The von Mises stress reached its maximum value near the inner radius, increasing from approximately 98 MPa at $\omega$ = 150 rad/s to approximately 279 MPa at $\omega$ = 250 rad/s. Comparison with ANSYS simulations demonstrated excellent agreement, confirming the validity of the analytical formulation. Furthermore, the developed ANN model accurately reproduced the stress distributions with $R^2$ values above 0.998 and prediction errors below 0.36%.

These findings indicate that machine learning can provide a reliable and computationally efficient alternative for rapid stress estimation and preliminary design optimization of rotating hybrid structures operating under thermo-mechanical loading conditions. The analytical, numerical, and ANN results showed excellent agreement, demonstrating the reliability of the proposed framework for rapid stress prediction and design assessment of hybrid rotating cylinders.

### Author Contributions

“Conceptualization, Hüseyin Fırat Kayıran; methodology, Hüseyin Fırat Kayıran; software, Hüseyin Fırat Kayıran; validation, Hüseyin Fırat Kayıran; formal analysis, Hüseyin Fırat Kayıran; investigation, Hüseyin Fırat Kayıran; resources, Hüseyin Fırat Kayıran; data curation, Hüseyin Fırat Kayıran; writing—original draft preparation, Hüseyin Fırat Kayıran; writing—review and editing, Hüseyin Fırat Kayıran; visualization, Hüseyin Fırat Kayıran; supervision, Hüseyin Fırat Kayıran; project administration, Hüseyin Fırat Kayıran. The author has read and agreed to the published version of the manuscript.”

### Funding

"This research has not received any external funding"

### Data Availability Statement

The article does not report any data.

### Conflicts of Interest

There are no known competing financial interests or personal relationships that could have influenced the work reported in this article.

**Acknowledgement**

I would like to express my gratitude to my wife, for her constant support during my work.

**References**

[1] Thakur, P., & Gulial, P. (2025). Thermal and mechanical behavior of natural rubber and polystyrene cylinder s under edge-loading. Journal of Rubber Research, 28, 493–504. https://doi.org/10.1007/s42464-025-00316-3

[2] Soni, A., Das, P. K., Kumar, S., Mishra, V., Pagare, A., Kumar, D., & Kumar, S. (2023). Tribological characterizations of thermoplastic composites. Materials Today: Proceedings, 79(1), 92–99. https://doi.org/10.1016/j.matpr.2022.09.231

[3] Sahu, R. K., Panda, S. K., & Dash, P. (2022). Stress analysis of rotating functionally graded cylinders. Journal of Research in Engineering and Science & Management, 5(4), 71–79.

[4] Al-Furjan, M. S. H., Habibi, M., Safarpour, H., & Sharifpour, A. (2022). Kevlar fiber reinforced composites: A review. Journal of Materials Research and Technology, 18, 477–505.

[5] Goyal, A., Gupta, M., & Singh, S. (2023). Mechanical behavior of carbon–aramid hybrid composites. Composites Part B: Engineering, 247, 110308.

[6] Lee, S., Shin, D., Kim, G., & Ji, W. (2022). Hybrid thermoplastic composite modeling. Composites Part C: Open Access, 7, 100215. https://doi.org/10.1016/j.jcomc.2021.100215

[7] Eldeeb, A. M., Shabana, Y. M., & Elsawaf, A. (2023). Thermoelastic stress mitigation in rotating discs. Journal of Strain Analysis for Engineering Design, 58(8). https://doi.org/10.1177/03093247231165091

[8] Zhang, Y., Liu, X., & Wang, J. (2021). Machine learning-based stress prediction in composite structures. Composite Structures, 270, 114089.

[9] Liu, H., Chen, Z., & Zhao, Y. (2022). Data-driven modeling for rotating systems. Engineering Applications of Artificial Intelligence, 113, 104902.

[10] Kayiran, H. F. (2025). Machine learning-based investigation of stress in carbon fiber rotating cylinders. Knowledge and Decision Systems With Applications, 1, 1–10. https://doi.org/10.59543/kadsa.v1i.13519

[11] Fırat Kayıran, H. (2025). Machine learning-assisted thermo-elastic analysis of fiber-reinforced composite rotating cylinder s. Intelligent Systems Research and Applications Journal, 1, 1–12. https://doi.org/10.59543/ctg7te95

[12] Kayıran, H. F. (2026). Thermo-elastic analysis of an axisymmetric layered cylinder under constant thermal loading with artificial intelligence-based validation. Intelligent Systems Research and Applications Journal, 2, 76–89. https://doi.org/10.59543/0x8ky937

[13] Kayıran, H. F. (2026). Physics-informed machine learning for predicting thermomechanical stress in rotating carbon-aramid hybrid composites. Knowledge and Decision Systems With Applications, 2, 408–421. https://doi.org/10.59543/rpwq1n92

[14] Reddy, J. N. (2013). An introduction to continuum mechanics (2nd ed.). Cambridge University Press.

[15] Boley, B. A., & Weiner, J. H. (1960). Theory of thermal stresses. Wiley.

[16] Hetnarski, R. B., & Eslami, M. R. (2009). Thermal stresses: Advanced theory and applications. Springer.

[17] Lamé, G. (1852). Leçons sur la théorie mathématique de l'élasticité des corps solides. Bachelier.

[18] Bower, A. F. (2009). Applied mechanics of solids. CRC Press.

[19] Timoshenko, S. P., & Goodier, J. N. (1970). Theory of elasticity (3rd ed.). McGraw-Hill.

[20Hands-On Machine Learning with Scikit-Learn, Keras, and TensorFlow, Géron, A. (2022). *Hands-On Machine Learning with Scikit-Learn, Keras, and TensorFlow* (3rd ed.). O'Reilly Media.

[21] Ashby, M. F. (2011). Materials selection in mechanical design (4th ed.). Butterworth-Heinemann.

[22] Sadd, M. H. (2014). Elasticity: Theory, applications, and numerics (3rd ed.). Academic Press.

[23] Sheikhi, A., Khoshbakhti Saray, R., Shafiei Ghazani, A., Geimechi, A., & Lashkarpour, S. M. (2026). Thermal management and optimization of a 6-cylinder heavy-duty diesel engine: A two-way coupled CFD, FEA and combustion numerical study. Fuel, 405(Part C), 136634. https://doi.org/10.1016/j.fuel.2025.136634

[24] Jin, Q., Jiang, W., Jia, C., & Ma, J. (2026). Residual stress control in nozzle to cylinder butt welds of large-scale pressure vessels using primary plus secondary local PWHT method. Journal of Pressure Vessel Technology, 148(4), 041502. https://doi.org/10.1115/1.4071201

[25] Jin, Q., Jiang, W., Ma, J., Jia, C., Wu, A., & Wu, C. (2025). Experimental and numerical analysis of residual stress relief mechanisms of local postweld heat treatment in pressure vessels. Thin-Walled Structures, 211, 112487. https://doi.org/10.1016/j.tws.2024.112487

[26] Yang, B., Yu, H., Jiang, W., Gu, W., & Chen, J. (2024). Stress relief simulation for post-weld heat treatment process of pressure equipment: Creep constitutive equation considering temperature and stress variations. International Journal of Pressure Vessels and Piping, 208, 105156. https://doi.org/10.1016/j.ijpvp.2024.105156

[27] Niu, S., Li, X., Liu, C., Li, L., Han, T., & Han, B. (2024). Study on low temperature and narrow heating bands of post weld heat treatment for girth welds stress reduction of long-distance pipelines. International Journal of Pressure Vessels and Piping, 212, 105347. https://doi.org/10.1016/j.ijpvp.2024.105347

[28] Bhutada, A., Kumar, S., Gunasegaram, D., & Alankar, A. (2021). Machine learning based methods for obtaining correlations between microstructures and thermal stresses. Metals, 11(8), 1167. https://doi.org/10.3390/met11081167

[29] Zhu, C., et al. (2023). Numerical simulation and optimization with artificial neural network of two-phase nanofluid flow in a circular heatsink with cylindrical pin-fins. Engineering Analysis with Boundary Elements, 148, 305–316.

[30] Jabbari, M., Sohrabpour, S., & Eslami, M. R. (2002). Mechanical and thermal stresses in a functionally graded hollow cylinder due to radially symmetric loads. International Journal of Pressure Vessels and Piping, 79(7), 493–497.

[31] Liew, K. M., Kitipornchai, S., Zhang, X., & Lim, C. W. (2003). Analysis of the thermal stress behaviour of functionally graded materials. International Journal of Solids and Structures.